### Title

Energy Landscape of Molecular Motion in Cubic Methylammonium Lead Iodide from First-Principles




### Journal

The Journal of Physical Chemistry C, 120(23)

### ISSN

1932-7447 1932-7455



### Authors

Bechtel, Jonathon S
Seshadri, Ram
Van der Ven, Anton



### Publication Date

2016-06-16

### DOI

10.1021/acs.jpcc.6b03570

Peer reviewed

# Energy Landscape of Molecular Motion in Cubic Methylammonium Lead Iodide from First Principles

Jonathon S. Bechtel,[†] Ram Seshadri,[†,‡] and Anton Van der Ven[*,†]

*Materials Department, University of California, Santa Barbara, Santa Barbara, CA 93106, and Department of Chemistry and Biochemistry, and Materials Research Laboratory, University of California, Santa Barbara, Santa Barbara, CA 93106*

E-mail: avdv@engineering.ucsb.edu

[*]To whom correspondence should be addressed

[†]Materials Department, University of California, Santa Barbara, Santa Barbara, CA 93106

[‡]Department of Chemistry and Biochemistry, and Materials Research Laboratory, University of California, Santa Barbara, Santa Barbara, CA 93106

**Abstract**

Molecular $A$-cation dynamics are known to play a role in the electronic properties and structure of hybrid organic-inorganic $ABX_3$ perovskites such as $CH_3NH_3PbI_3$. We calculate the full energy landscape for rigid-body rotations and translations of the methylammonium cation in the cubic phase of $CH_3NH_3PbI_3$. Energy barriers are calculated for combinations of molecular reorientation, on-axis rotation, and molecular translation within the unit cell. Allowing molecular translations significantly stabilizes orientations along [100] which we attribute to strong N−H$\cdots$I interactions between $CH_3NH_3^+$ and the inorganic Pb−I host lattice.

# Introduction

Hybrid organic-inorganic perovskite materials for photovoltaics present a promising avenue toward efficient, inexpensive solar energy conversion.[1] Reaching power conversion efficiencies of nearly 20%, the record-setting perovskites consist of a Pb−I octahedral framework with methylammonium cations ($CH_3NH_3^+$) occupying the $A$-site.[2–4] Long electron-hole diffusion lengths,[5,6] high absorption coefficients,[7,8] and a 1.6 eV band gap[7,9] contribute to the remarkable photovoltaic properties of this material.

Establishing structure-property relationships in $CH_3NH_3PbI_3$ has proven challenging due to important entropic contributions arising from $PbI_6$ octahedral tilting and $CH_3NH_3^+$ rotational degrees of freedom. At elevated temperature, the $PbI_6$ octahedra of the inorganic host undergo large tilt-mode oscillations relative to their average positions in the ideal cubic structure,[10] while the molecular cations rotate rapidly.[11,12] Distortions of the inorganic lattice by halide substitution and octahedral tilting have been shown to influence the band gap and absorption properties.[7,13–15] Although the $A$-cation does not contribute to electronic states near the band gap,[16–18] it has been shown to affect the nature of the band gap through interaction with the inorganic Pb−I sublattice.[19] Moreover, the dielectric properties of $CH_3NH_3PbI_3$ are linked to both the rotational dynamics and ordering of the molecular $A$-

cation and the structural phase transitions of the inorganic Pb−I lattice.[11,20–23]

$CH_3NH_3PbI_3$ undergoes a transition from the high-temperature pseudo-cubic aristotype $Pm\bar{3}m$ structure to the tetragonal $I4/mcm$ phase ($a^0a^0c^-$ tilt system in Glazer notation)[24] at 330 K and then to the orthorhombic $Pnma$ phase ($a^+b^-c^-$ tilt system) below 160 K.[25–28] The transitions associated with $A$-cation ordering have been the subject of some debate.[11–13,20,29–31] Nevertheless, recent quasi-elastic neutron scattering experiments indicate that the $CH_3NH_3^+$ molecules in the cubic phase dynamically disorder and undergo both fast reorientations of the C−N bond axis (≈5 ps at 300 K) and faster on-axis rotations about the C−N bond axis (≈1 ps at 300 K).[11] Some degrees of freedom freeze out upon cooling and only on-axis rotations are observed in the low temperature orthorhombic phase (≈4 ns at 70 K) accompanied by a dramatic loss in dielectric permittivity.[11]

Several studies have employed first-principles calculations to reveal the microscopic origins of preferential $CH_3NH_3^+$ orientations and the interactions between $CH_3NH_3^+$ and the inorganic Pb−I host lattice.[32,33] In the orthorhombic phase, energy barriers of ≈100 meV were calculated for on-axis rotations of the staggered configuration of $CH_3NH_3^+$ due to strong N−H$\cdots$I interactions, suggesting fully ordered $A$-cations in the low temperature phase.[32] Recently, $CH_3NH_3^+$ rotations were investigated in the tetragonal phase, and energy barriers of ≈50 and ≈20 meV for on-axis rotation were found depending on the molecular orientation.[33] While past studies have explored the energy of the crystal for a subset of orientations and on-axis rotational degrees of freedom, an understanding of the interactions of the $A$-cation with the inorganic Pb−I sublattice as a function of all its rotational and translational degrees of freedom remains incomplete.

In this letter, we map out the full energy landscape of $CH_3NH_3^+$ motion in the cubic inorganic host by accounting for all reorientations of the C−N bond axis, all on-axis rotations about the bond axis, and translations of the molecule from the ideal $A$-site. While the orthorhombic phase is characterized by ordered $CH_3NH_3^+$ orientations in a rigid host lattice, large anharmonic vibrational excitations associated with octahedral tilting and disordered

molecular orientations and translations add considerable structural complexity to the high-temperature cubic phase. Here we focus on the ideal cubic perovskite structure in order to investigate the microscopic details of N−H interactions with the Pb−I host lattice. We find that the energy of the crystal is especially sensitive to molecular translations which lead to a stabilization of the [100] orientation as a result of favorable N−H$\cdots$I interactions. The energy barriers to reorientation approach 100 meV when translations are considered, while barriers to on-axis rotations range from 200 meV in the [111] orientation to <10 meV in the [110] and [100] orientations. Finally, we show that molecular orientation has minimal effect on the band structure. In contrast, distortions of the inorganic Pb−I lattice in response to different orientations and translations of $CH_3NH_3^+$ can cause as much as a 0.25 eV increase in the band gap and, additionally, can change it from direct to indirect.

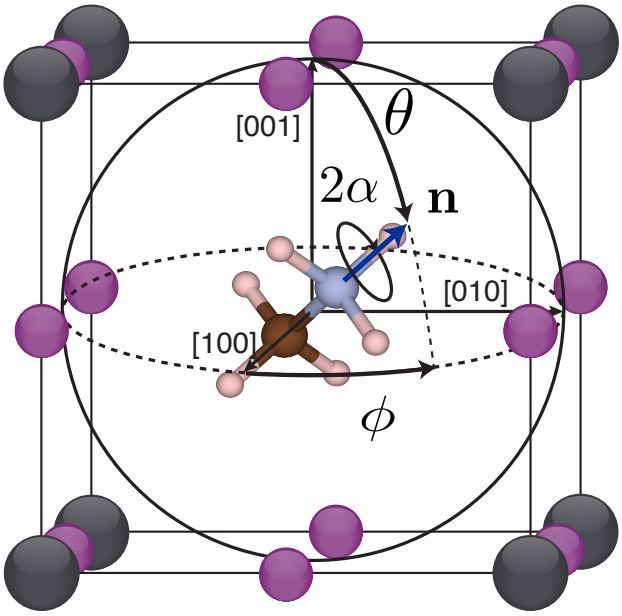


Figure 1: Molecular rotational degrees of freedom described by the axis-angle representation. Orientation of the C−N bond axis is given by $\mathbf{n}(\phi, \theta)$, and on-axis rotations are described by the angle $2\alpha$ about the bond axis.

# Methods

Energies associated with molecular rotation were calculated with density functional theory (DFT) as implemented in the Vienna ab initio Simulation Package (VASP)[34,35] using projector augmented wave[34,36] (PAW) pseudopotentials within the Perdew-Burke-Ernzerhof (PBE) generalized gradient approximation (GGA).[37] Approximate van der Waals corrections were accounted for with the zero damping DFT-D3 method of Grimme.[38] For the cubic aristotype a 6×6×6 $k$-point mesh centered at the Γ point was employed with a 700 eV plane wave energy cutoff. Energies were converged to within 1 meV/atom with respect to $k$-point density. A volume relaxation of the cubic parent phase resulted in an optimized lattice parameter of 6.32 Å which agrees very well with the experimental lattice parameter 6.3286 Å at 343 K.[26] The methylammonium cation geometry and bond lengths were adapted from experimental and computational structures of the orthorhombic phase at 100 K.[28,32] The final molecular geometry was obtained by relaxing the molecular cation geometrically centered on the cubic perovskite $A$-site with a staggered H arrangement, and this geometry was fixed throughout all subsequent rigid-body rotations and translations. Crystal structures were visualized using the VESTA program suite.[39]

# Results and Discussion

We define molecular rotations with respect to a reference configuration where the C−N bond axis is oriented in the [100] direction of the cubic host. As shown in Figure 1, the rotational degrees of freedom can be described by the axis-angle representation where the polar angle $\theta$ and the azimuthal angle $\phi$ define an orientation vector for the C−N bond. This vector also serves as a rotation axis, with $2\alpha$ denoting the rotation angle around the C−N bond. The inclination of the molecule from the $xy$ plane is given by $|\theta - \pi/2|$ while the azimuthal angle, $\phi$, describes the counterclockwise rotation around the $z$-axis. For $\theta = 90°$ and $\phi = 45°$ the molecular C−N axis points toward the edge of the cubic unit cell in the [110] direction,

while $\theta = 54.74°$, $\phi = 45°$ corresponds to a molecular orientation along the body diagonal of the cubic unit cell in the [111] direction.

The Kohn-Sham energy landscapes of molecular rotations were calculated in an ideal cubic perovskite crystal structure which corresponds to the average high temperature (>330K) phase observed in $CH_3NH_3PbI_3$. In addition to molecular rotations we also considered translation of the *A*-cation within the cage formed by the $PbI_6$ octahedra. Due to the cubic symmetry of the perovskite structure, it is sufficient to consider only orientations within the region enclosed by the [100], [110], and [111] crystallographic directions, which we will refer to as the asymmetric region in orientation space. The 48 symmetry operations of the *Oh* point group tile the asymmetric region over the complete orientation space. We calculated the energies associated with on-axis rotations and translations of up to 1.0 Å in the direction of the N atom over a grid that spanned the asymmetric region of orientation space.

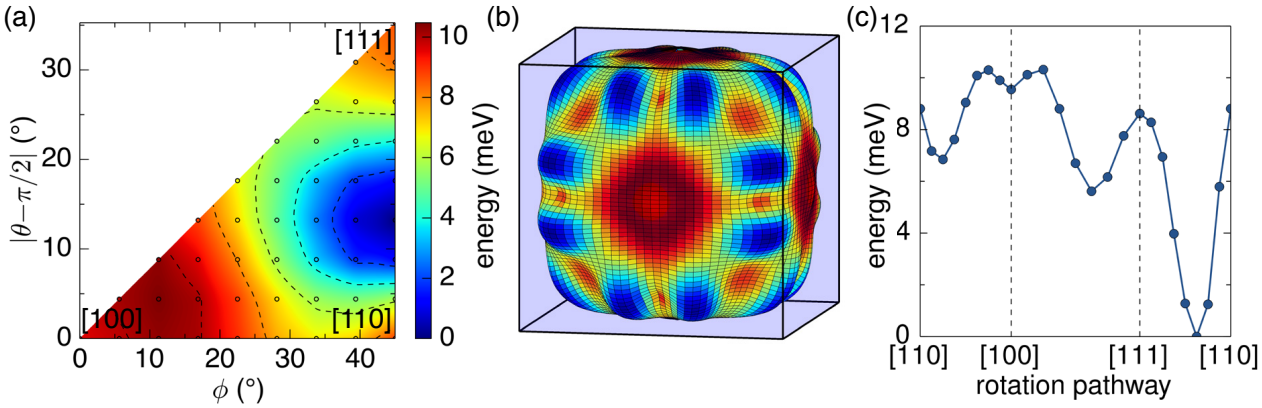


Figure 2: (a) Interpolated energy surfaces for molecular reorientation of $CH_3NH_3^+$ within cubic $PbI_6$ octahedral cages where the molecular geometrical center of mass resides at the *A*-site. At each orientation, the energy corresponding to the minimum energy on-axis rotation is plotted. (b) Polar plot of orientational energy surface where the radius is proportional to $|E - \beta E_{\max}|$ of scale from (a) where $\beta = 1 - {}^1/_{1000}$. (c) Energies for selected rotational pathways along the edges of the aymmetric orientation region which represent rotations within the (001) and $(\bar{1}10)$ lattice planes via [100] → [110] and [001] → [111] → [110] rotations, respectively.

To probe the strength and nature of the interactions between the molecular *A*-cation and the inorganic Pb−I sublattice, we first consider the energy surface associated with the ideal cubic structure with the molecule's geometric center of mass located at the ideal

perovskite $A$-site. The calculated energy surface is shown in Figure 2(a,b). The minimum energy surface for the centered molecule is constructed by considering the minimum energy on-axis rotation, $2\alpha$, of $CH_3NH_3^+$ at each orientation ($\theta$,$\phi$). In this way, the minimum energy surface for the space of all rigid body rotations is considered at zero translation. Figure 2c reveals a shallow energy surface for the centered molecule in which any reorientation is met by a small energy barrier $<$11 meV. Thus, the molecular $A$-cation should tumble freely above room temperature if its position is restricted to the center of the cubic inorganic cage.

However, when translations of $CH_3NH_3^+$ are taken into account, as shown in Figure 3(a,b,c) for the three high-symmetry molecular orientations, it becomes clear that the center of the perovskite $A$-site cage is not the lowest energy configuration for the molecular cation. Instead, translation in any positive direction (in the direction of the ammonium group) lowers the energy. Due to the point group of the molecule, all energy surfaces obey the symmetries of $C_3$; therefore only on-axis rotations up to 120° need be considered. In the [100] direction (Figure 3a), minima occur for a 0.6 Å translation toward the face of the cubic unit cell while on-axis rotations remarkably have no effect on the energy surface. In the [110] and [111] directions, however, the energy does depend strongly on both molecular translations and on-axis rotations. When oriented toward the edge of the cubic unit cell along the [110] direction (Figure 3b), the molecular cation favors a 0.3 Å translation with two equivalent low-energy rotational configurations. Similarly, in the [111] orientation (Figure 3c), the $A$-cation tends to off-center by 0.4 Å, and adopts a preferred rotational configuration aligned with proximal I atoms. The locus of minimum energy translations are summarized in Figure 4, which depicts off-centering preferences toward the face of the cubic unit cell and along the body diagonal.

We attribute the tendencies to off center and to adopt specific rotational states to N$-$H$\cdots$I hydrogen-bonding interactions. For instance, at a translation of 0.4 Å in the [111] direction, the local minimum observed in Figure 3c corresponds to near alignment and N$-$H$\cdots$I distances of approximately 2.6 Å. In contrast, the local maximum along the 0.4 Å translation for the same direction corresponds to an on-axis rotation that maximizes

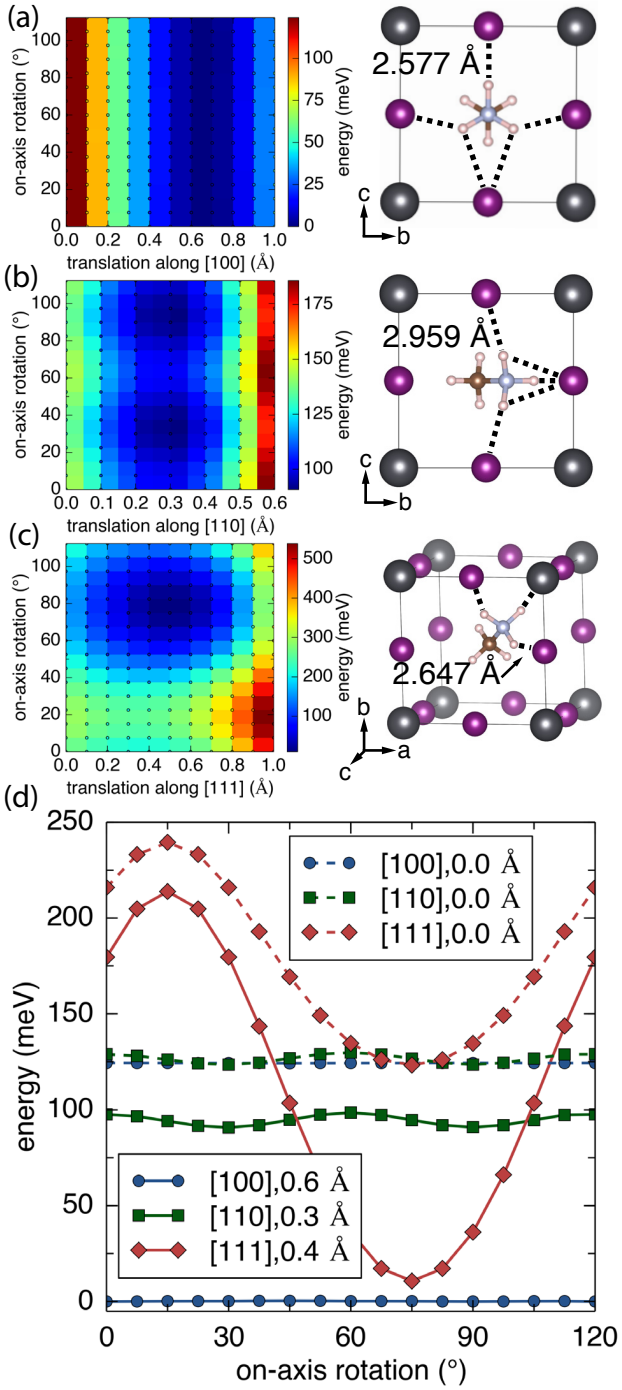


Figure 3: (a,b,c) Energy surfaces plotted as heat maps for the three high symmetry directions showing the effect of molecular translation and twisting rotations. Energy heat maps (a,b,c) share the same absolute energy scale but are shown with relative color scales. Low energy configurations in each high symmetry orientation are shown with the minimum N−H···I distance labeled. (d) Relative energies associated with on-axis rotations at zero translation and the minimum energy translation in each direction.

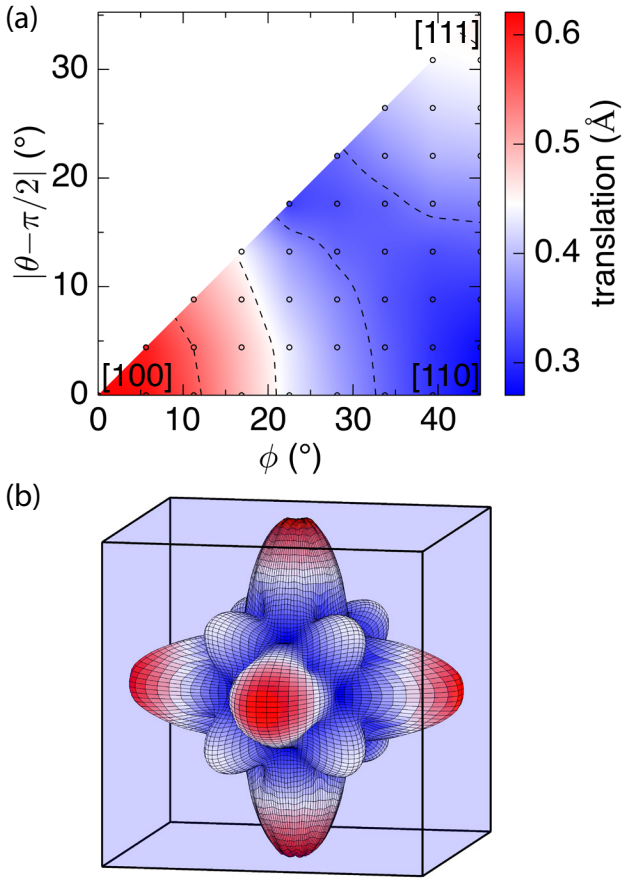


Figure 4: (a) Within the asymmetric orientation region, the translations associated with the lowest energy configurations are plotted. The inclination and azimuthal angles are given relative to the [100] reference configuration. (b) Polar plot where the radius is proportional to the minimum-energy translation providing a representation of the locus of minimum energy molecular translations throughout the cubic unit cell.

N−H···I distances. The effect of on-axis rotations decreases from the [111], [110] to [100] directions as shown in Figure 3d. Along the body-diagonal of the cubic unit cell, on-axis rotations which minimize N−H···I distances are stabilized by 203 meV compared to the rotation that maximizes N−H···I distances. On the other hand, on-axis rotations only account for a 7 meV energy decrease in the [110] direction, and, in the [100] direction, there is no preferred on-axis rotation. These differences stem from the number of favorable N−H···I interactions for the different orientation geometries. Along [111] (Figure 3c), the molecule can simultaneously minimize three N−H···I distances (2.64 Å); thus on-axis rotations en-

counter a large energy penalty as these three interactions are all simultaneously disrupted. Along [110] (Figure 3b), the energy is lowered by only two minimized N−H$\cdots$I distances (2.96 Å). Hence, when the molecule rotates it is able to form a new N−H$\cdots$I bond as it breaks two old ones resulting in a lower energy barrier to on-axis rotations. Lastly, in the [100] orientation (Figure 3a), only one N−H$\cdots$I is minimized at a time (2.58 Å), so upon on-axis rotation, a favorable N−H$\cdots$I interaction is reformed as soon as an old one is broken, resulting in an extremely shallow energy profile. These trends show that the differences in calculated energy barriers to on-axis rotation between the high-symmetry orientations stem from the number of disrupted N−H$\cdots$I interactions.

Figure 5(a,b,c) shows the energy as a function of orientation ($\theta$, $\phi$), after minimizing not only over on-axis rotations, but also over translational degrees of freedom. A comparison with Figure 2, where translations were not treated as a degree of freedom, reveals the significant impact that molecular off-centering from the *A*-site has on the crystal energy. Molecular transitions between two locally stable configurations require reorientation, translation and an axial rotation. The most favored directions are in the [100] and [111] orientations, separated by high energy barriers to reorientation. Figure 5c, for example, shows that the reorientation from [110] to [100] (corresponding to molecular rotation in the (001) plane) encounters a 100 meV energy barrier. For the molecule to reorient between the [100] and [111] directions it must surmount an 85 meV energy barrier, while an 80 meV energy barrier separates the [110] and [111] orientations. Hence, a molecule rotating within the $(\bar{1}10)$ plane from the $z$-axis, through [111] to [110] and $[11\bar{1}]$ to the negative $z$-axis encounters a maximum barrier of 85 meV. Moreover, Figure 5 shows the large stabilization of the [100] direction when translations are considered, which is a result of reduced N−H$\cdots$I distances. In particular, the energies for the low-energy configurations in the high-symmetry directions decrease as the N−H$\cdots$I distances decrease from 2.96 Å for the [110] orientation to 2.65 Å along [111] and to 2.58 Å along [100], resulting in relative energies $E_{\rm min}^{[110]} > E_{\rm min}^{[111]} > E_{\rm min}^{[100]}$. Thus as identified above, the number of N−H$\cdots$I interactions dictates the barrier to on-axis rotation,

but $CH_3NH_3^+$ orientational preferences originate from minimizing N−H$\cdots$I distances.

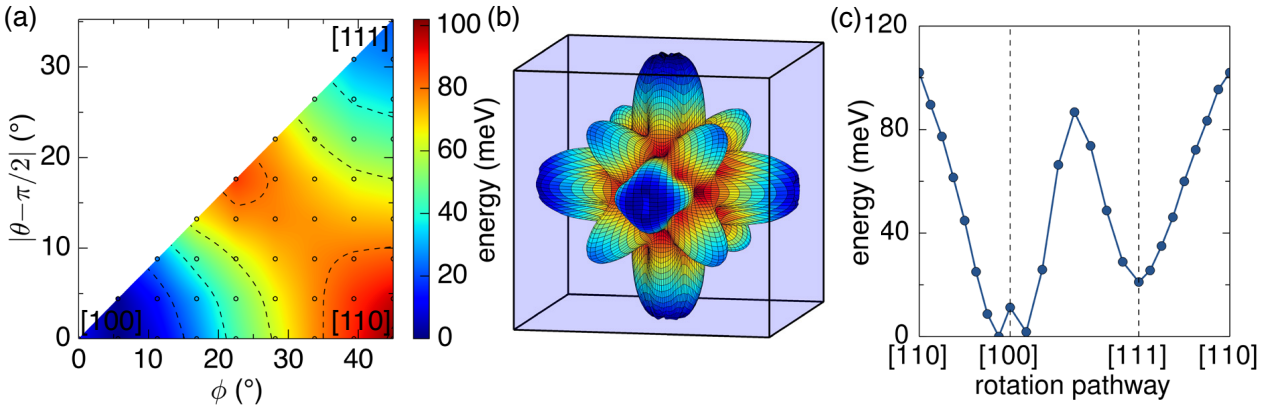


Figure 5: (a) Interpolated energy surfaces for molecular reorientation of $CH_3NH_3^+$ within cubic $PbI_6$ octahedral cages. At each orientation, the energy corresponding to the minimum energy on-axis rotation and minimum-energy translation is plotted. (b) Polar plot of orientational energy surface where the radius is proportional to $|E - \beta E_{\max}|$ of scale from (a) where $\beta = 1 - {}^1/_{1000}$. (c) Energies for selected rotational pathways along the edges of the asymmetric orientation region which represent rotations within the (001) and $(\bar{1}10)$ lattice planes via [100] → [110] and [001] → [111] → [110] rotations, respectively.

We also investigated the electronic band structure as a function of molecular orientation to assess the impact of molecular rotation on the electronic properties of $CH_3NH_3PbI_3$. It is well known that Pb 6*s* and I 5*p* $\sigma$-antibonding orbitals form the top of the valence band while Pb 6*p* and I 5*p* $\pi$-antibonding orbitals contribute to the bottom of the conduction band.[40] The calculated atomic orbital contributions to the electronic density of states in Figure 6a confirm the participation of Pb *s* and I *p* orbitals in the valence band as well as Pb *p* and I *p* orbital contributions to the conduction states. Therefore, the inorganic Pb−I host lattice dictates the electronic properties of the $CH_3NH_3PbI_3$ perovskite. This is verified by the calculated electronic band structures for the three high-symmetry $CH_3NH_3^+$ orientations in a cubic $PbI_3$ host shown in Figure 6a. The almost perfectly overlapping band structures in Figure 6a reveal that molecular orientation plays a minimal role in determining the nature of the bands near the band gap.

Pb-containing compounds often exhibit interesting lone pair chemistry which typically manifests in high Born effective charges indicating a tendency for Pb off-centering and the

formation of local dipoles.[41,42] The calculated Born effective charge tensors for the $Pb^{2+}$ ions of cubic $CH_3NH_3PbI_3$ is predicted to be nearly isotropic with values of the averaged trace around $4.9\,e$. Well above the nominal value of $+2\,e$, the high values for the Born effective charges suggest a highly polarizable Pb $s$-lone pair. Figure 6(b,c,d), showing the summed partial charge density near the top of the valence bands, reveals the interplay between the molecular dipole and the Pb $s$-lone pair. As is evident in Figure 6(b,c,d), the orientation of the $A$-cation affects the charge density surrounding the Pb atoms. In fact in the cubic perovskite, an asymmetry arises in the Pb valence electron distribution, with the Pb valence states tending to polarize in opposition to the molecular orientation. Due to the periodic boundary conditions imposed in our calculations, it must be recognized that the partial charge density represents that of a crystal with periodically aligned organic cations in a ferro arrangement, where the orientation, translation, and on-axis rotations are repeated periodically throughout the crystal. The presence of such ferroelectric domains at ambient temperature is an intensely debated topic. Several studies[43–45] suggest that ferroelectric domains exist at room temperature and aid carrier separation through internal electric fields while others[46,47] observe no appreciable macroscopic polarization. While the reported partial charge densities may not represent operating conditions at high-temperatures due to the artificial periodic boundary conditions, in the presence of an applied electric field, $CH_3NH_3PbI_3$ does exhibit macroscopic polarization.[47] In this context, the predicted high $Pb^{2+}$ Born effective charges and the sensitivity of the Pb valence charge on molecular orientation suggests that the Pb $s$-lone pair plays a role in the polarizability and dielectric response of $CH_3NH_3PbI_3$.

The high-temperature $CH_3NH_3PbI_3$ cubic phase is stabilized by vibrational entropy and experiences large oscillations of the inorganic octahedral network, with root-mean-squared atomic displacements as high as 0.41 Å for the I-sublattice in the direction perpendicular to the Pb−I−Pb bond.[10] Hence, while the calculated rigid-body rotational energy landscape (Figure 5) corresponds to $CH_3NH_3^+$ motion within the average cubic structure with nominal 180° Pb−I−Pb bond angles, the local $A$-site environments of the actual crystal fluctuate

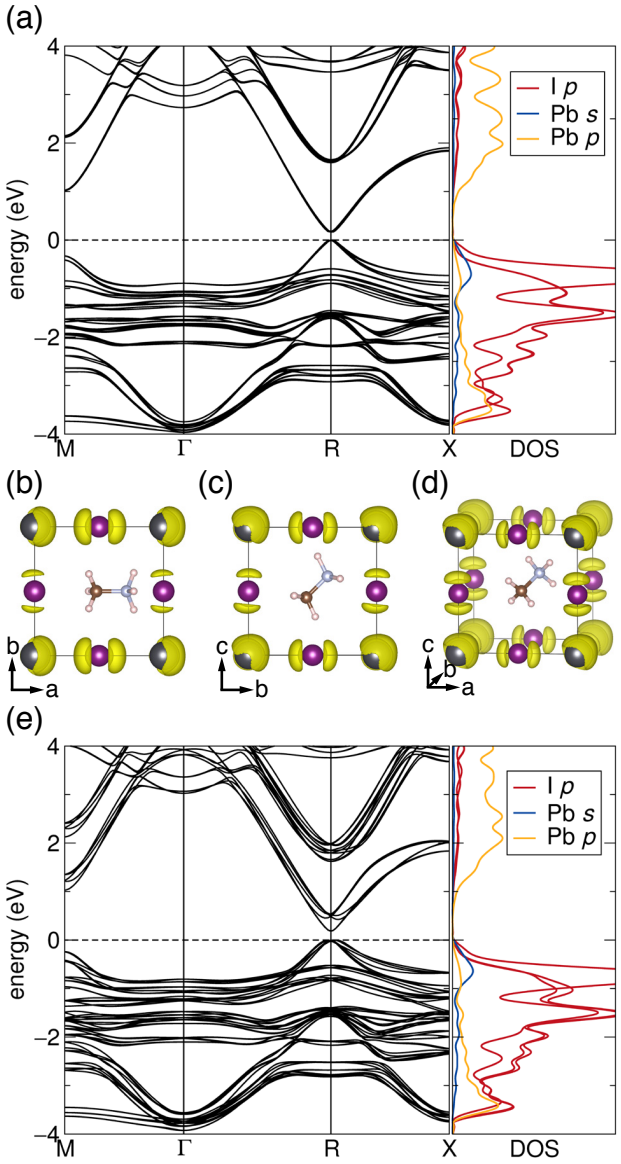


Figure 6: (a) Overlayed band structures for high symmetry molecular orientations in the ideal cubic perovskite depicting the direct band gap at the $R$ point in GGA-PBE with spin-orbit coupling. DOS presented for the lowest energy [100] orientation. (b,c,d) Partial charge density associated with top of the valence band for the high symmetry directions ([100], [110], [111]), showing the Pb $s$ and I $p$ orbital character at isosurface levels of $1.912 \times 10^{-5}$, $1.925 \times 10^{-5}$ and $1.920 \times 10^{-5}$ $e/\text{Å}^3$, respectively. (e) Overlayed band structures for the three high symmetry molecular orientations after relaxing only the inorganic lattice. DOS shown for relaxed [100] orientation.

freely as a result of I-sublattice displacements at finite temperature (>330 K).

The true energy landscape of the solid is substantially more complex than that probed in this study. It depends not only on the rotational and translational degrees of freedom of $CH_3NH_3^+$, but also on the displacement degrees of freedom of the Pb and I host atoms. Collective octahedral tilting degrees of freedom are especially important as they are in part responsible for the symmetry breaking phase transformations upon cooling[25–28] and likely dominate the anharmonic vibrational excitations that stabilize the high temperature cubic phase. Mapping out this more complex energy landscape can be done with an effective Hamiltonian[48–53] that is expressed as a function of displacement degrees of freedom of the inorganic host along with the rotational and translational degrees of freedom of the $A$-cation. High temperature behavior as well as low temperature symmetry breaking orderings can then be probed with Monte Carlo simulations.

While a full statistical mechanics study relying on an effective Hamiltonian is beyond the scope of this work, we can nevertheless obtain a sense of the coupling between displacement degrees of freedom of the $PbI_3$ host and the orientational and translational degrees of freedom of $CH_3NH_3^+$ by considering relaxations of the host for different rigid molecular orientations and translations. To this end, we performed DFT relaxations in which the internal degrees of freedom of the inorganic lattice (within a fixed cubic unit cell) were allowed to relax to forces less than 5 meV/ Å while the molecular cation was held rigidly in place. Both the Pb and I-sublattices experience significant distortions from the ideal cubic aristotype as shown in Figure 7(a,b,c) where the N−H$\cdots$I distances as well as Pb−I−Pb angles are labeled to emphasize the relevant distortions.

The most significant distortions are observed for the [110] orientation (Figure 7b) with 164° Pb−I−Pb bond angles. Similarly, in the relaxed [100] configuration (Figure 7a), Pb−I−Pb bond angles of 168° are found. The observed I-sublattice displacements support the idea that N−H$\cdots$I interactions play a dominant role in stabilizing the preferred molecular orientations.

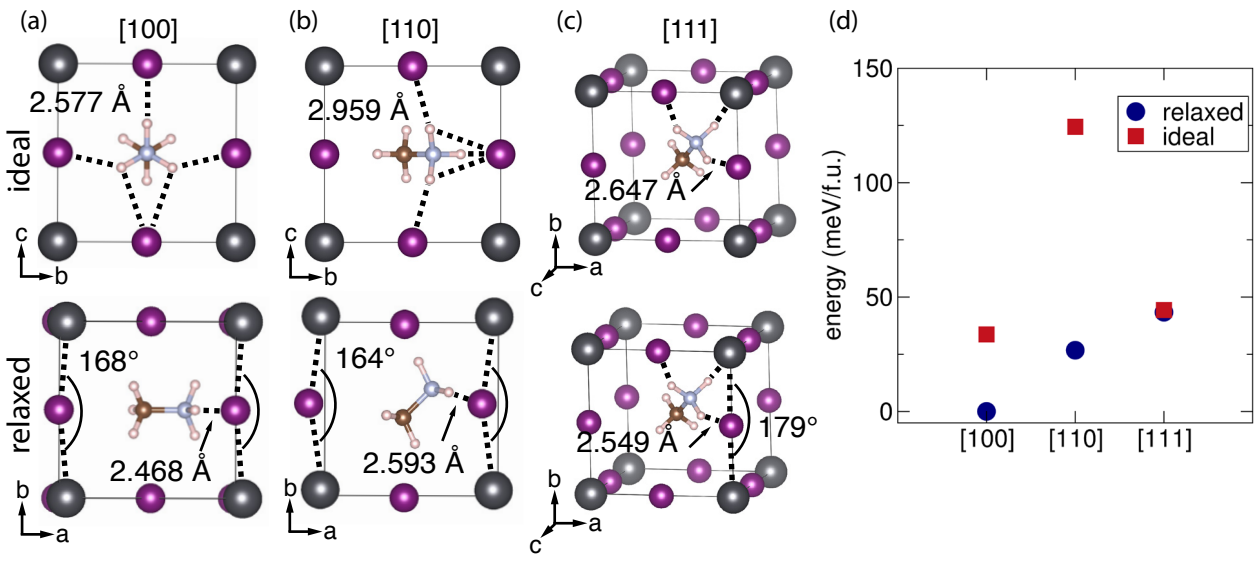


Figure 7: (a,b,c) Ideal (cubic) and relaxed inorganic lattice around rigid $CH_3NH_3^+$ molecules in the [100],[110], and [111] directions, respectively. (d) Relative energy comparison per formula unit of the ideal and relaxed configurations for each of the three high-symmetry orientations.

Relaxation of Pb and I around a rigid $CH_3NH_3^+$ molecule also has a dramatic effect on the electronic band structure of the material. Figure 6e, shows the calculated electronic band structures corresponding to configurations with relaxed Pb and I ions. Since the inorganic Pb−I host lattice governs the electronic properties of $CH_3NH_3PbI_3$, distortions in the Pb−I−Pb bond angle directly impact the band structure near the band gap. The distortions of the inorganic cage widen the band gap by almost 0.25 eV, and the nature of the band gap changes from direct to indirect, which has been previously identified as a factor leading to an increase in minority carrier lifetime and to the suppression of radiative recombination.[19]

In summary, we have calculated the energy surface of $CH_3NH_3PbI_3$ as a function of the orientational, translational and on-axis rotational degrees of freedom of $CH_3NH_3^+$ within the *A*-site cage of the cubic Pb−I perovskite host. Our calculations show that N−H$\cdots$I interactions play a dominant role in determining low energy $CH_3NH_3^+$ orientations and translations. The energy landscape as a function of molecular orientation when minimized over translational and on-axis rotational degrees of freedom is highly anisotropic, a property

that should be accounted for in meso-scale models of this compound. Translational degrees of freedom are found to be especially important with the equilibrium translations exhibiting a strong dependence on molecular orientation. Molecular reorientation in cubic Pb−I will therefore require substantial rigid translation when following the minimum energy surface. We also found that the band structure of cubic $CH_3NH_3PbI_3$ is relatively insensitive to the *A*-cation orientation, but can change substantially when the Pb−I host is allowed to relax in response to different configurations of $CH_3NH_3^+$. In addition to revealing the nature of the interactions between $CH_3NH_3^+$ and the inorganic perovskite host, the results of this work set the stage for future statistical mechanics studies relying on effective Hamiltonians to probe the finite temperature vibrational, rotational and translational excitations and their effect on electronic structure in this fascinating class of materials.

## Acknowledgement

This material is based upon work supported by the National Science Foundation, Grant DMR-1410242. RS gratefully acknowledges support from the U.S. Department of Energy, Office of Science, Basic Energy Sciences under award number DE-SC-0012541. JSB thanks Dr. John C. Thomas and Douglas Fabini for helpful discussions. Computational resources provided by the National Energy Research Scientific Computing Center (NERSC), supported by the Office of Science and U.S. Department of Energy, under Contract DE-AC02-05CH11231, are gratefully acknowledged in addition to support from the Center for Scientific Computing at the CNSI and MRL: an NSF MRSEC (DMR-1121053), National Science Foundation CNS-0960316, and Hewlett Packard.

## References

(1) Lee, M. M.; Teuscher, J.; Miyasaka, T.; Murakami, T. N.; Snaith, H. J. Efficient Hybrid Solar Cells Based on Meso-Superstructured Organometal Halide Perovskites. *Science* **2012**, *338*, 643–647.

(2) Zhou, H.; Chen, Q.; Li, G.; Luo, S.; Song, T.-b.; Duan, H.-S.; Hong, Z.; You, J.; Liu, Y.; Yang, Y. Interface Engineering of Highly Efficient Perovskite Solar Cells. *Science* **2014**, *345*, 542–546.

(3) Jeon, N. J.; Noh, J. H.; Kim, Y. C.; Yang, W. S.; Ryu, S.; Seok, S. I. Solvent Engineering for High-Performance Inorganic-Organic Hybrid Perovskite Solar Cells. *Nature Mater.* **2014**, *13*, 897–903.

(4) Yang, W. S.; Noh, J. H.; Jeon, N. J.; Kim, Y. C.; Ryu, S.; Seo, J.; Seok, S. I. High-Performance Photovoltaic Perovskite Layers Fabricated through Intramolecular Exchange. *Science* **2015**, *348*, 1234–1237.

(5) Stranks, S. D.; Eperon, G. E.; Grancini, G.; Menelaou, C.; Alcocer, M. J. P.; Leijtens, T.; Herz, L. M.; Petrozza, A.; Snaith, H. J. Electron-Hole Diffusion Lengths Exceeding 1 Micrometer in an Organometal Trihalide Perovskite Absorber. *Science* **2013**, *342*, 341–344.

(6) Xing, G.; Mathews, N.; Sun, S.; Lim, S. S.; Lam, Y. M.; Grätzel, M.; Mhaisalkar, S.; Sum, T. C. Long-Range Balanced Electron- and Hole-Transport Lengths in Organic-Inorganic $CH_3NH_3PbI_3$. *Science* **2013**, *342*, 344–347.

(7) Kojima, A.; Teshima, K.; Shirai, Y.; Miyasaka, T. Organometal Halide Perovskites as Visible-Light Sensitizers for Photovoltaic Cells. *J. Am. Chem. Soc.* **2009**, *131*, 6050–6051.

(8) De Wolf, S.; Holovsky, J.; Moon, S. J.; Löper, P.; Niesen, B.; Ledinsky, M.; Haug, F. J.; Yum, J. H.; Ballif, C. Organometallic Halide Perovskites: Sharp Optical Absorption Edge and its Relation to Photovoltaic Performance. *J. Phys. Chem. Lett.* **2014**, *5*, 1035–1039.

(9) Kim, H.-S.; Lee, C.-R.; Im, J.-H.; Lee, K.-B.; Moehl, T.; Marchioro, A.; Moon, S.-J.; Humphry-Baker, R.; Yum, J.-H.; Moser, J. E. et al. Lead Iodide Perovskite Sensitized

All-Solid-State Submicron Thin Film Mesoscopic Solar Cell with Efficiency Exceeding 9%. *Sci. Rep.* **2012**, *2*, 591.

(10) Kawamura, Y.; Mashiyama, H.; Hasebe, K. Structural Study on Cubic-Tetragonal Transition of $CH_3NH_3PbI_3$. *J. Phys. Soc. Japan* **2002**, *71*, 1694–1697.

(11) Chen, T.; Foley, B. J.; Ipek, B.; Tyagi, M.; Copley, J. R.; Brown, C. M.; Choi, J. J.; Lee, S.-H. Rotational Dynamics of Organic Cations in the $CH_3NH_3PbI_3$ Perovskite. *Phys. Chem. Chem. Phys.* **2015**, *17*, 31278–31286.

(12) Bakulin, A. A.; Selig, O.; Bakker, H. J.; Rezus, Y. L.; Müller, C.; Glaser, T.; Lovrincic, R.; Sun, Z.; Chen, Z.; Walsh, A. et al. Real-Time Observation of Organic Cation Reorientation in Methylammonium Lead Iodide Perovskites. *J. Phys. Chem. Lett.* **2015**, *6*, 3663–3669.

(13) Mosconi, E.; Quarti, C.; Ivanovska, T.; Ruani, G.; De Angelis, F. Structural and Electronic Properties of Organo-Halide Lead Perovskites: A Combined IR-Spectroscopy and Ab Initio Molecular Dynamics Investigation. *Phys. Chem. Chem. Phys.* **2014**, *16*, 16137–16144.

(14) Kulkarni, S. A.; Baikie, T.; Boix, P. P.; Yantara, N.; Mathews, N.; Mhaisalkar, S. Band-gap Tuning of Lead Halide Perovskites Using a Sequential Deposition Process. *J. Mater. Chem. A* **2014**, *2*, 9221–9225.

(15) Amat, A.; Mosconi, E.; Ronca, E.; Quarti, C.; Umari, P.; Nazeeruddin, M. K.; Grätzel, M.; De Angelis, F. Cation-Induced Band-Gap Tuning in Organohalide Perovskites: Interplay of Spin-Orbit Coupling and Octahedra Tilting. *Nano Lett.* **2014**, *14*, 3608–3616.

(16) Brivio, F.; Butler, K. T.; Walsh, A.; Van Schilfgaarde, M. Relativistic Quasiparticle Self-Consistent Electronic Structure of Hybrid Halide Perovskite Photovoltaic Absorbers. *Phys. Rev. B* **2014**, *89*, 155204.

(17) Umari, P.; Mosconi, E.; De Angelis, F. Relativistic GW Calculations on $CH_3NH_3PbI_3$ and $CH_3NH_3SnI_3$ Perovskites for Solar Cell Applications. *Sci. Rep.* **2014**, *4*, 4467.

(18) Yin, W.-J.; Shi, T.; Yan, Y. Unusual Defect Physics in $CH_3NH_3PbI_3$ Perovskite Solar Cell Absorber. *Appl. Phys. Lett.* **2014**, *104*, 063903.

(19) Motta, C.; El-Mellouhi, F.; Kais, S.; Tabet, N.; Alharbi, F.; Sanvito, S. Revealing the Role of Organic Cations in Hybrid Halide Perovskite $CH_3NH_3PbI_3$. *Nature Commun.* **2015**, *6*, 7026.

(20) Leguy, A. M. A.; Frost, J. M.; McMahon, A. P.; Sakai, V. G.; Kochelmann, W.; Law, C.; Li, X.; Foglia, F.; Walsh, A.; O'Regan, B. C. et al. The Dynamics of Methylammonium Ions in Hybrid Organic-Inorganic Perovskite Solar Cells. *Nature Commun.* **2015**, *6*, 7124.

(21) Fabini, D. H.; Hogan, T.; Evans, H. A.; Stoumpos, C. C.; Kanatzidis, M. G.; Seshadri, R. Dielectric and Thermodynamic Signatures of Low-Temperature Glassy Dynamics in the Hybrid Perovskites $CH_3NH_3PbI_3$ and $HC(NH_2)_2PbI_3$. *J. Phys. Chem. Lett.* **2016**, *7*, 376–381.

(22) Labram, J. G.; Fabini, D. H.; Perry, E. E.; Lehner, A. J.; Wang, H.; Glaudell, A. M.; Wu, G.; Evans, H.; Buck, D.; Cotta, R. et al. Temperature-Dependent Polarization in Field-Effect Transport and Photovoltaic Measurements of Methylammonium Lead Iodide. *J. Phys. Chem. Lett.* **2015**, *6*, 3565–3571.

(23) Poglitsch, A.; Weber, D. Dynamic Disorder in Methylammoniumtrihalogenoplumbates (II) Observed by Millimeter-Wave Spectroscopy. *J. Chem. Phys.* **1987**, *87*, 6373–6378.

(24) Glazer, A. M. The Classification of Tilted Octahedra in Perovskites. *Acta Crystallogr. Sect. B Struct. Crystallogr. Cryst. Chem.* **1972**, *28*, 3384–3392.

(25) Baikie, T.; Fang, Y.; Kadro, J. M.; Schreyer, M.; Wei, F.; Mhaisalkar, S. G.; Gratzel, M.; White, T. J. Synthesis and Crystal Chemistry of the Hybrid Perovskite $(CH_3NH_3)PbI_3$ for Solid-State Sensitised Solar Cell Applications. *J. Mater. Chem. A* **2013**, *1*, 5628–5641.

(26) Baikie, T.; Barrow, N. S.; Fang, Y.; Keenan, P. J.; Slater, P. R.; Piltz, R. O.; Gutmann, M.; Mhaisalkar, S. G.; White, T. J. A Combined Single Crystal Neutron/X-ray Diffraction and Solid-State Nuclear Magnetic Resonance Study of the Hybrid Perovskites $CH_3NH_3PbX_3$ (X = I, Br and Cl). *J. Mater. Chem. A* **2015**, *3*, 9298–9307.

(27) Stoumpos, C. C.; Malliakas, C. D.; Kanatzidis, M. G. Semiconducting Tin and Lead Iodide Perovskites with Organic Cations: Phase Transitions, High Mobilities, and Near-Infrared Photoluminescent Properties. *Inorg. Chem.* **2013**, *52*, 9019–9038.

(28) Weller, M. T.; Weber, O. J.; Henry, P. F.; Di Pumpo, M.; Hansen, T. C. Complete Structure and Cation Orientation in the Perovskite Photovoltaic Methylammonium Lead Iodide between 100 and 352 K. *Chem. Commun.* **2015**, *51*, 4180–4183.

(29) Even, J.; Carignano, M.; Katan, C. Molecular Disorder and Translation/Rotation coupling in the Plastic Crystal Phase of Hybrid Perovskites. *Nanoscale* **2015**, *8*, 6222–6236.

(30) Mattoni, A.; Filippetti, A.; Saba, M. I.; Delugas, P. Methylammonium Rotational Dynamics in Lead Halide Perovskite by Classical Molecular Dynamics: The Role of Temperature. *J. Phys. Chem. C* **2015**, *119*, 17421–17428.

(31) Carignano, M. A.; Kachmar, A.; Hutter, J. Thermal Effects on $CH_3NH_3PbI_3$ Perovskite from Ab Initio Molecular Dynamics Simulations. *J. Phys. Chem. C* **2015**, *119*, 8991–8997.

(32) Lee, J.-H.; Bristowe, N. C.; Bristowe, P. D.; Cheetham, A. K. Role of Hydrogen-Bonding and its Interplay with Octahedral Tilting in $CH_3NH_3PbI_3$. *Chem. Commun.* **2015**, *51*, 6434–6437.

(33) Lee, J. H.; Lee, J.-H.; Kong, E.-H.; Jang, H. M. The Nature of Hydrogen-Bonding Interaction in the Prototypic Hybrid Halide Perovskite, Tetragonal $CH_3NH_3PbI_3$. *Sci. Rep.* **2016**, *6*, 21687.

(34) Kresse, G.; Furthmüller, J. Efficient Iterative Schemes for Ab Initio Total-Energy Calculations Using a Plane-Wave Basis Set. *Phys. Rev. B* **1996**, *54*, 11169–11186.

(35) Kresse, G. From Ultrasoft Pseudopotentials to the Projector Augmented-Wave Method. *Phys. Rev. B* **1999**, *59*, 1758–1775.

(36) Blöchl, P. E. Projector Augmented-Wave Method. *Phys. Rev. B* **1994**, *50*, 17953.

(37) Perdew, J. P.; Burke, K.; Ernzerhof, M. Generalized Gradient Approximation Made Simple. *Phys. Rev. Lett.* **1996**, *77*, 3865–3868.

(38) Grimme, S.; Antony, J.; Ehrlich, S.; Krieg, H. A Consistent and Accurate Ab Initio Parametrization of Density Functional Dispersion Correction (DFT-D) for the 94 Elements H-Pu. *J. Chem. Phys.* **2010**, *132*, 154104.

(39) Momma, K.; Izumi, F. VESTA: A Three-Dimensional Visualization System for Electronic and Structural Analysis. *J. Appl. Crystallogr.* **2008**, *41*, 653–658.

(40) Umebayashi, T.; Asai, K.; Kondo, T.; Nakao, A. Electronic Structures of Lead Iodide Based Low-Dimensional Crystals. *Phys. Rev. B* **2003**, *67*, 155405.

(41) Brgoch, J.; Lehner, A. J.; Chabinyc, M. L.; Seshadri, R. Ab Initio Calculations of Band Gaps and Absolute Band Positions of Polymorphs of $RbPbI_3$ and $CsPbI_3$: Implications for Main-Group Halide Perovskite Photovoltaics. *J. Phys. Chem. C* **2014**, *18*, 27721–27727.

(42) Waghmare, U.; Spaldin, N.; Kandpal, H.; Seshadri, R. First-Principles Indicators of Metallicity and Cation Off-centricity in the IV-VI Rocksalt Chalcogenides of Divalent Ge, Sn, and Pb. *Phys. Rev. B* **2003**, *67*, 125111.

(43) Kutes, Y.; Ye, L.; Zhou, Y.; Pang, S.; Huey, B. D.; Padture, N. P. Direct Observation of Ferroelectric Domains in Solution-Processed $CH_3NH_3PbI_3$ Perovskite Thin Films. *J. Phys. Chem. Lett.* **2014**, *5*, 3335–3339.

(44) Chen, H.-W.; Sakai, N.; Ikegami, M.; Miyasaka, T. Emergence of Hysteresis and Transient Ferroelectric Response in Organo-Lead Halide Perovskite Solar Cells. *J. Phys. Chem. Lett.* **2014**, *6*, 164–169.

(45) Chen, B.; Shi, J.; Zheng, X.; Zhou, Y.; Zhu, K.; Priya, S. Ferroelectric Solar Cells Based on Inorganic-Organic Hybrid Perovskites. *J. Mater. Chem. A* **2015**, *3*, 7699–7705.

(46) Beilsten-Edmands, J.; Eperon, G. E.; Johnson, R. D.; Snaith, H. J.; Radaelli, P. G. Non-Ferroelectric Nature of the Conductance Hysteresis in $CH_3NH_3PbI_3$ Perovskite-Based Photovoltaic Devices. *Appl. Phys. Lett.* **2015**, *106*, 173502.

(47) Coll, M.; Gomez, A.; Mas-Marza, E.; Almora, O.; Garcia-Belmonte, G.; Campoy-Quiles, M.; Bisquert, J. Polarization Switching and Light-Enhanced Piezoelectricity in Lead Halide perovskites. *J. Phys. Chem. Lett.* **2015**, *6*, 1408–1413.

(48) Rabe, K. M.; Waghmare, U. V. Localized Basis for Effective Lattice Hamiltonians: Lattice Wannier Functions. *Phys. Rev. B* **1995**, *52*, 13236–13246.

(49) Thomas, J. C.; Van der Ven, A. Finite-Temperature Properties of Strongly Anharmonic and Mechanically Unstable Crystal Phases from First Principles. *Phys. Rev. B* **2013**, *88*, 214111.

(50) Zhong, W.; Vanderbilt, D.; Rabe, K. M. First-Principles Theory of Ferroelectric Phase Transitions for Perovskites: The Case of $BaTiO_3$. *Phys. Rev. B* **1995**, *52*, 6301–6312.

(51) Mueller, T.; Ceder, G. Effective Interactions between the N-H Bond Orientations in Lithium Imide and a Proposed Ground-State Structure. *Phys. Rev. B* **2006**, *74*, 134104.

(52) Drautz, R.; Fähnle, M. Spin-Cluster Expansion: Parametrization of the General Adiabatic Magnetic Energy Surface with Ab Initio Accuracy. *Phys. Rev. B* **2004**, *69*, 104404.

(53) Bhattacharya, J.; Van der Ven, A. Mechanical Instabilities and Structural Phase Transitions: The Cubic to Tetragonal Transformation. *Acta Mater.* **2008**, *56*, 4226–4232.

# Graphical TOC Entry